This article has been accepted for publication in a future issue of this journal, but has not been fully edited. Content may change prior to final publication.
DOI: 10.17775/CSEEJPES.2022.06570

Real-time Harmonic Contribution Evaluation Considering Multiple Dynamic Customers

Shaohua Yang, *Student Member, IEEE,* Keng-Weng Lao, *Senior Member, IEEE,* Hongxun Hui, *Member, IEEE,* Yulin Chen, *Member, IEEE,* and Ningyi Dai, *Senior Member, IEEE*

***Abstract*—The widespread deployment of renewable energies and non-linear loads has led to serious harmonic pollution in the electrical distribution networks. Evaluation of the harmonic contribution (HC) of each customer is a significant task for power quality management. Most previous studies focus on periodic evaluation methods, where numerous data have to be collected in advance over a period (e.g., one day). However, customer behaviors are time-varying and would lead to dynamic HCs, which can not be captured by traditional periodic evaluation methods. To address this issue, this paper presents a novel real-time HC evaluation method considering multiple dynamic customers. First, a two-stage iteration estimator is proposed based on the information fusion technique to quantify the real-time HC of each customer. Then, to mitigate the negative effect of unknown background harmonics, a dominant index method is developed to determine the credibility of the measurement data. On this basis, an adaptive gain selection strategy is proposed to improve the accuracy of real-time HC evaluation. By doing so, the major harmonic contributor can be identified for implementing harmonic suppression and improving power quality. Finally, a typical IEEE system is utilized to verify the proposed methods. The results show that using the proposed method, the evaluation errors can be reduced from about 10% to 2.5%. Moreover, the total harmonic distortion of voltage can be suppressed from 5.564% to 0.702%. Therefore, this research can be helpful for guiding harmonic problems in power systems.**

***Index Terms*—Power quality, harmonic contribution, dynamic customer behavior, background harmonic, real-time evaluation.**

I. Introduction

RENEWABLE energies and non-linear loads [1] (e.g., wind generations [2], inverter-based air conditioners [3], electric vehicles, etc.) are growing rapidly in the modern power system [4]–[6]. As a consequence, the harmonic sources are widely dispersed throughout the electrical distribution network, which leads to more serious harmonic pollution [7]. Compared conventional generators, harmonic sources are characterized by widespread distribution and deep coupling, which makes the harmonic problem complicated [8]. In order to enhance harmonic management (in particular, to implement harmonic suppression measures), it is important to identify the major harmonic sources first [9]. This problem is generally named harmonic contribution (HC) evaluation.

There have been extensive studies conducted in the field of HC evaluation. The existing methods are carried out from two perspectives, i.e., single-point HC evaluation and multi-point HC evaluation. The single-point HC evaluation aims at dividing the harmonic pollution responsibility between an individual customer and the main grid. However, due to widely distributed harmonic sources in the distribution network [10], multi-point HC evaluation emerges and becomes a worldwide research hotspot. The problem of multi-point HC evaluation can be illustrated by a distribution network, as shown in Fig. 1. In the network, multiple customers (i.e., harmonic sources) are connected with the point of common coupling (PCC)[1]. The objective of this problem is to quantify each customer's HC for the harmonic pollution according to the measurement data (i.e., harmonic voltages U_h^{PCC} and currents I_h^i) [11].

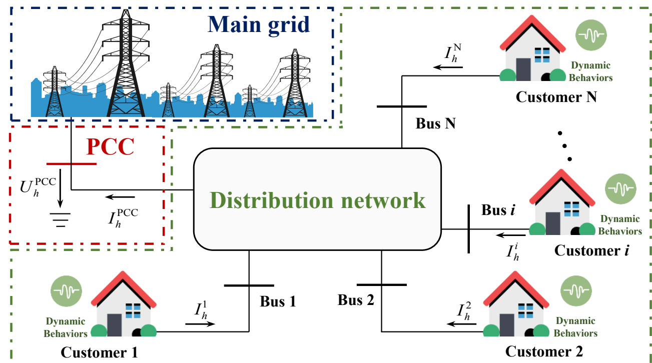

Fig. 1. A typical distribution network with multiple harmonic customers.

Previous methods can be broadly classified into two categories, i.e., invasive methods and non-invasive methods [12]–[23]. The invasive methods can obtain HC results from the voltage and current variations caused by additional injected harmonics or a known serial impedance connection, which may have harmful effects on the distribution network [12], [13]. For example, invasive methods may result in additional harmonic voltage and current disturbances or undesired changes in the network structure, which is harmful to the power systems [14]. In severe cases, invasive methods can lead to harmonic instability problems (e.g., harmonic resonance and low frequency oscillation), which degrade the power quality of the distribution network and can further deteriorate the stability and safety of power systems [15]–[17]. Due to these adverse effects, non-invasive methods are more suitable for the problem with multi-point harmonic customers, since instead of putting additional disturbances to the network, non-invasive methods utilize natural voltage and current variations over a period of time [18]. Non-invasive methods include the

This work was partly funded by The Science and Technology Development Fund, Macau SAR (File/Project no. SKL-IOTSC-2021-2023, 0003/2020/AKP, FDCT/0022/2020/A1). (Corresponding author: Keng-Weng Lao, Yulin Chen.)

S. Yang, K. Lao, H. Hui, Y. Chen and N. Dai are with the State Key Laboratory of Internet of Things for Smart City and Department of Electrical and Computer Engineering, University of Macau, Macao, 999078 China (email: yc17436@um.edu.mo, johnnylao@um.edu.mo, hongxunhui@um.edu.mo, chenyl2017@zju.edu.cn, nydai@um.edu.mo).

[1]PCC is the bus between the main grid and the distribution network, which is usually installed by devices to monitor the network's operating states.

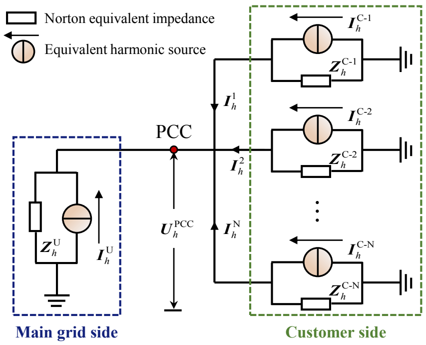

Fig. 2. Norton equivalent circuit of a network with multiple customers.

least square correlation method, the multiple linear regression method [19], the widely linear partial least squares method [20], and the complex least squares regression method (CLSR) [21]. In addition, the statistical methods based on the harmonic load profile are also effective when the number of measurements is larger than the number of harmonic sources [22], [23]. These methods are based on the assumption that background harmonics (BHs)[2] can keep stable during the periodic data collection, while this assumption may be infeasible in practice. Because the harmonic sources in the main grid are changing with time and there is a deep coupling between the harmonic sources [24]. Therefore, the BH fluctuations should be considered for the HC evaluation.

The independent component analysis method [25], complex independent component method [26], and data selection method [27] are employed to address the BH fluctuations for the HC evaluation problem [28]. However, these methods need periodic data collection (e.g., one day) to get natural variation information, which cannot reflect dynamic harmonic characteristics [29]. In modern distribution networks, new harmonic characteristics are arising, which should be taken into account in the HC evaluation. For example, because of the random and time-varying properties of renewable energies [30], [31], harmonics have more obvious fluctuations and dynamic characteristics [32]. Moreover, during the sampling period of time, customer behaviors (e.g., work or not, working modes, and different strategies of the inverter) may change several times [33]. As a result, the evaluation results based on the periodic sampling data cannot indicate the actual HC level. Therefore, a real-time evaluation method is needed to represent these dynamic HCs.

To the best of our knowledge, there is no published work to address the real-time HC evaluation considering multiple dynamic customers and BHs. To this end, we propose a real-time evaluation method with adaptive capabilities according to BHs. The major contributions of this paper are threefold:

1) A two-stage iteration estimator is proposed to reflect dynamic customer harmonic characteristics. With this estimator, the HC at the time of measurement can be evaluated immediately.
2) A dominant index method is developed to determine the credibility of the real-time measurement data, which can mitigate the negative effect caused by BHs.
3) An adaptive gain selection strategy is proposed according to the credibility of the measurement data. By doing so, the accuracy of HC evaluation can be improved.

[2]BHs are harmonics that come from non-linear components in the main grid.

The remainder of this paper is organized as follows. The model of the HC evaluation problem is presented in Section II. Then the real-time HC evaluation method is proposed in Section III. Numerical studies are presented in Section IV. Finally, Section V concludes this paper.

II. Modelling of Harmonic Contribution

Fig. 2 shows the Norton equivalent circuit of a distribution network with multiple customers. The symbol h indicates the harmonic order; $\boldsymbol{I}_h^U$ and $\boldsymbol{I}_h^{C-i}$ are equivalent current sources of the main grid and each customer, respectively; $\boldsymbol{Z}_h^U$ and $\boldsymbol{Z}_h^{C-i}$ are Norton equivalent impedance of the main grid and each customer, respectively. The harmonic voltage at the PCC is the vector sum of the harmonic voltages generated by customers and the BH voltage, so the h-th harmonic voltage at the PCC can be calculated as:

$$\begin{aligned}\boldsymbol{U}_h^{\mathrm{PCC}} =& \ \boldsymbol{Z}_h^{1-\mathrm{PCC}}\boldsymbol{I}_h^1 + \boldsymbol{Z}_h^{2-\mathrm{PCC}}\boldsymbol{I}_h^2 + \cdots + \boldsymbol{Z}_h^{i-\mathrm{PCC}}\boldsymbol{I}_h^i \\ &+ \cdots + \boldsymbol{Z}_h^{\mathrm{N}-\mathrm{PCC}}\boldsymbol{I}_h^{\mathrm{N}} + \boldsymbol{U}_h^{\mathrm{BH}} \\ =& \ \sum\nolimits_{i\in\mathcal{I}} \boldsymbol{Z}_h^{i-\mathrm{PCC}}\boldsymbol{I}_h^i + \boldsymbol{Z}_h^{\mathrm{BH}}\boldsymbol{I}_h^{\mathrm{BH}}, \ \forall i\in\mathcal{I}, \ \forall h\in\mathcal{H},\end{aligned} \tag{1}$$

where $\boldsymbol{I}_h^i$ is the h-th harmonic current to the PCC of customer i; $\boldsymbol{Z}_h^{i-\mathrm{PCC}}$ is the h-th harmonic transfer impedance between $\boldsymbol{I}_h^i$ and $\boldsymbol{U}_h^{\mathrm{PCC}}$; $\boldsymbol{U}_h^{\mathrm{BH}}$ and $\boldsymbol{I}_h^{\mathrm{BH}}$ are voltage and current of the BH at the PCC, respectively; $\boldsymbol{Z}_h^{\mathrm{BH}}$ is the harmonic transfer impedance for BH. $\mathcal{I}$ represents the set of N suspicious harmonic customers; $\mathcal{H}$ represents the set of all the considered harmonic orders.

For a group of historical measurement data (e.g., M is the number of samples) collected during a periodic time, the unknown parameters, including harmonic transfer impedance and the BH voltage in (1) can be estimated by the regression model as follows:

$$\begin{bmatrix}\boldsymbol{U}_h^{\mathrm{PCC}}(t_1) & \cdots & \boldsymbol{U}_h^{\mathrm{PCC}}(t_m) & \cdots & \boldsymbol{U}_h^{\mathrm{PCC}}(t_{\mathrm{M}})\end{bmatrix}^{\mathrm{T}} \tag{2}$$

$$= \begin{bmatrix}\boldsymbol{I}_h^1(t_1) & \cdots & \boldsymbol{I}_h^i(t_1) & \cdots & \boldsymbol{I}_h^{\mathrm{N}}(t_1) & 1 \\ \vdots & \ddots & \vdots & \ddots & \vdots & \\ \boldsymbol{I}_h^1(t_m) & \cdots & \boldsymbol{I}_h^i(t_m) & \cdots & \boldsymbol{I}_h^{\mathrm{N}}(t_m) & 1 \\ \vdots & \ddots & \vdots & \ddots & \vdots & \\ \boldsymbol{I}_h^1(t_{\mathrm{M}}) & \cdots & \boldsymbol{I}_h^i(t_{\mathrm{M}}) & \cdots & \boldsymbol{I}_h^{\mathrm{N}}(t_{\mathrm{M}}) & 1\end{bmatrix} \begin{bmatrix}\boldsymbol{Z}_h^{1-\mathrm{PCC}} \\ \vdots \\ \boldsymbol{Z}_h^{i-\mathrm{PCC}} \\ \vdots \\ \boldsymbol{Z}_h^{\mathrm{N}-\mathrm{PCC}} \\ \boldsymbol{U}_h^{\mathrm{BH}}\end{bmatrix},$$

where the operator $[\ ]^{\mathrm{T}}$ represents matrix conjugate transpose. Then by projecting $\boldsymbol{U}_h^i$ on $\boldsymbol{U}_h^{\mathrm{PCC}}$, the HCs of each customer and the BH can be quantified as follows:

$$\begin{aligned}\rho_h^i &= \frac{|\boldsymbol{U}_h^i| \ cos(\phi_h^i - \phi_h^{\mathrm{PCC}})}{|\boldsymbol{U}_h^{\mathrm{PCC}}|} \times 100\% \\ &= \frac{\boldsymbol{U}_h^i \cdot \boldsymbol{U}_h^{\mathrm{PCC}}}{|\boldsymbol{U}_h^{\mathrm{PCC}}|^2} \times 100\%, \ \forall i\in\mathcal{I}, \ \forall h\in\mathcal{H},\end{aligned} \tag{3}$$

$$\rho_h^{\mathrm{BH}} = \left(1 - \sum\nolimits_{i\in\mathcal{I}} \rho_h^i\right) \times 100\%, \ \forall h\in\mathcal{H}, \tag{4}$$

where the operator $\cdot$ indicates dot product; $|\ |$ operator indicates modulus of vector; ρ_h^i and ρ_h^{BH} represent the harmonic contribution levels at the PCC of suspicious customers and the BH, respectively; ϕ_h^i and ϕ_h^{PCC} denote phase angles of $\boldsymbol{U}_h^i$ and $\boldsymbol{U}_h^{\mathrm{PCC}}$, respectively.

However, the HCs (i.e., ρ_h^i and ρ_h^{BH}) derived by the above periodic evaluation cannot capture actual dynamic HCs, since customer behaviors may change several times within the periodic time interval. To reflect the dynamic HCs of customers, we propose a real-time HC evaluation method, which is introduced in section III.

III. Real-time Evaluation of Harmonic Contribution

In order to achieve the real-time HC evaluation, a two-stage iteration estimator based on the information fusion technique is proposed at first, which can achieve HC evaluation results based on the real-time measurement, thus avoiding lengthy data collection time. This part is introduced in subsection III-A. In addition, to mitigate the negative effect caused by unknown BHs, a dominant index method is developed to determine the credibility of the real-time measurement data in subsection III-B. Finally, according to the credibility of the measurement data, an adaptive gain selection strategy is proposed by self-tuning parameters in subsection III-C to improve the accuracy of real-time evaluation.

A. Two-stage Iteration Estimator for Real-time HC Evaluation

The essential technique of the proposed estimator is to fuse the information from the state transition model and measurement model to obtain real-time HC evaluations close to the actual values, which is based on Kalman theorem. The problem of HC evaluation can be described by the state transition model and measurement model as follows:

$$\begin{cases} \boldsymbol{x}_k = \boldsymbol{A}_k \boldsymbol{x}_{k-1} + \boldsymbol{\omega}_{k-1} \\ \boldsymbol{z}_k = \boldsymbol{H}_k \boldsymbol{x}_k + \boldsymbol{\nu}_k \end{cases}, \ \forall k \in \mathcal{K}, \tag{5}$$

where $\boldsymbol{x}_k \in \mathbb{R}^n$ is the state vector at moment k; $\boldsymbol{A}_k$ is the $n \times n$ Markov transition matrix that relates to the state at the sampling moment $k-1$; $\boldsymbol{z}_k \in \mathbb{R}^m$ is the measurement vector; $\boldsymbol{H}_k$ is the observation matrix; $\boldsymbol{\omega}_{k-1}$ and $\boldsymbol{\nu}_k$ are the vector of random process and measurement error, respectively; $\mathcal{K}$ represents the set of sampling moments during the overall time of the HC evaluation. In our problem, the matrix $\boldsymbol{A}_k$ is set to the identity matrix since the distribution network is a quasi-steady state during a short period; $\boldsymbol{x}_k$ is the process state vector of harmonic transfer impedance and BH voltage, which can be expressed as follows:

$$\boldsymbol{x}_k = \begin{bmatrix} \boldsymbol{Z}_{h,k}^{1-\mathrm{PCC}} & \cdots & \boldsymbol{Z}_{h,k}^{i-\mathrm{PCC}} & \cdots & \boldsymbol{Z}_{h,k}^{\mathrm{N}-\mathrm{PCC}} & \boldsymbol{U}_{h,k}^{BH} \end{bmatrix}^{\mathrm{T}}, \\ \forall i \in \mathcal{I}, \forall k \in \mathcal{K}, \forall h \in \mathcal{H}. \tag{6}$$

In addition, the measurement vector $\boldsymbol{z}_k$ is the vector of the updated measured harmonic voltage at the PCC, which can be indicated as follows:

$$\boldsymbol{z}_k = \begin{bmatrix} \boldsymbol{U}_{h,k}^{\mathrm{PCC}} \end{bmatrix}, \ \forall k \in \mathcal{K}, \forall h \in \mathcal{H}. \tag{7}$$

The observation matrix $\boldsymbol{H}_k$ is the $m \times n$ matrix which can map the state $\boldsymbol{x}_k$ into the measurement $\boldsymbol{z}_k$ and can be given as follows:

$$\boldsymbol{H}_k = \begin{bmatrix} \boldsymbol{I}_{h,k}^1 & \boldsymbol{I}_{h,k}^2 & \cdots & \boldsymbol{I}_{h,k}^i & \cdots & \boldsymbol{I}_{h,k}^{\mathrm{N}} & 1 \end{bmatrix}, \\ \forall i \in \mathcal{I}, \forall k \in \mathcal{K}, \forall h \in \mathcal{H}. \tag{8}$$

The random process error $\boldsymbol{\omega}_k$ and the measurement error $\boldsymbol{\nu}_k$ are independent mutually with Gaussian white noises and can be denoted as follows:

$$\begin{cases} E[\boldsymbol{\omega}_k \boldsymbol{\omega}_s^{\mathrm{T}}] = \boldsymbol{Q}_k \delta \\ E[\boldsymbol{\nu}_k \boldsymbol{\nu}_s^{\mathrm{T}}] = \boldsymbol{R}_k \delta \\ E[\boldsymbol{\omega}_k \boldsymbol{\nu}_s^{\mathrm{T}}] = 0 \end{cases}, \begin{cases} p(\boldsymbol{\omega}_k) \sim N(0, \boldsymbol{Q}_k) \\ p(\boldsymbol{\nu}_k) \sim N(0, \boldsymbol{R}_k) \end{cases}, \tag{9}$$

where the $E[\ ]$ is the expectation operator; k and s represent two different sampling moments; $\boldsymbol{Q}_k$ and $\boldsymbol{R}_k$ represent the process and measurement error co-variance matrices, respectively, and they indicate the error degrees of the state transition model and measurement model, respectively; δ is the Dirac delta function, which can be shown as follows:

$$\delta = \begin{cases} 1, & k = s \\ 0, & k \neq s \end{cases}. \tag{10}$$

The two stages of the estimator are prior estimation and measurement correction, respectively.

1) *Prior Estimation*:

The first stage of the proposed two-stage estimator is the prior estimation, which can be achieved by using the state transition model and can be described as follows:

$$\hat{\boldsymbol{x}}_k^- = \boldsymbol{A}_k \boldsymbol{x}_{k-1}, \ \forall k \in \mathcal{K}, \tag{11}$$

where $\hat{\boldsymbol{x}}_k^-$ is the prior estimation from projecting the previous state.

2) *Measurement Correction*:

In the second stage, the prior estimation is corrected by the real-time measurement model to obtain a more accurate posterior estimation. The concept of an innovation matrix $\mathit{\Delta}_k^-$ is introduced and can be expressed as follows:

$$\mathit{\Delta}_k^- = \underbrace{\boldsymbol{z}_k}_{\text{measurement}} - \underbrace{\boldsymbol{H}_k \hat{\boldsymbol{x}}_k^-}_{\text{prior estimation}}, \ \forall k \in \mathcal{K}, \tag{12}$$

where $\mathit{\Delta}_k^-$ represents the new information that real-time measurement vector $\boldsymbol{z}_k$ brings to the prior estimation. The first term of the innovation matrix is related to measurement, and the second is related to the prior estimation. Based on the innovation matrix, the state transition model can be corrected by the measurement model timely, and the posterior estimation can be obtained as follows:

$$\hat{\boldsymbol{x}}_k = \hat{\boldsymbol{x}}_k^- + \boldsymbol{G}_k \mathit{\Delta}_k^-, \ \forall k \in \mathcal{K}, \tag{13}$$

where $\hat{\boldsymbol{x}}_k$ is the posterior estimation from both the state transition model and measurement model; $\boldsymbol{G}_k \in [\boldsymbol{0}, \boldsymbol{H}_k^-]$ is the $n \times m$ correction gain at the moment k. The larger correction gain means that prior results are corrected by the real-time measurement model more powerfully, and vice versa.

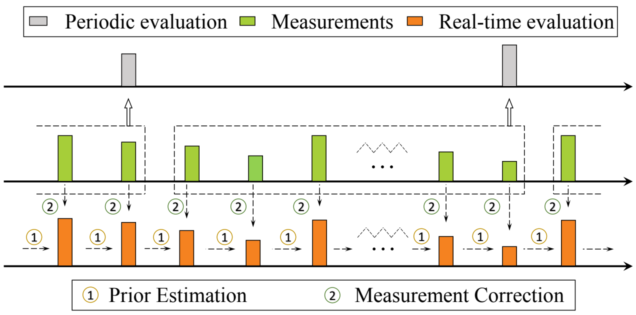

Fig. 3. The periodic evaluation and proposed real-time evaluation methods.

It is worth noting that the accurate posterior estimation can be obtained by properly adjusting the correction gain $\boldsymbol{G}_k$ of this two-stage estimator. To this end, posterior estimation error $\boldsymbol{e}_k$ is defined first as follows:

$$\boldsymbol{e}_k = \boldsymbol{x}_k - \hat{\boldsymbol{x}}_k, \ \forall k \in \mathcal{K}, \tag{14}$$

where $\boldsymbol{x}_k$ is the actual state value. Similar to (9), the error co-variance matrix $\boldsymbol{P}_k$ can be expressed as follows:

$$\begin{aligned}\boldsymbol{P}_k &= E[\boldsymbol{e}_k \boldsymbol{e}_k^{\mathrm{T}}] \\ &= \boldsymbol{P}_k^- - \boldsymbol{P}_k^- \boldsymbol{H}_k^T \boldsymbol{G}_k^T - \boldsymbol{G}_k \boldsymbol{H}_k \boldsymbol{P}_k^- + \boldsymbol{G}_k \boldsymbol{R}_k \boldsymbol{G}_k^T \\ &+ \boldsymbol{G}_k \boldsymbol{H}_k \boldsymbol{P}_k^- \boldsymbol{H}_k^T \boldsymbol{G}_k^T, \ \forall k \in \mathcal{K},\end{aligned} \tag{15}$$

where $\boldsymbol{P}_k^-$ is the co-variance matrix corresponding to the prior estimation error. Through achieving the objective of minimizing the error co-variance matrix $\boldsymbol{P}_k$, the posterior estimation can be corrected to the closest actual value. With this condition, the correction gain is designed as follows:

$$\boldsymbol{G}_k = \frac{\left(\boldsymbol{A}_k \boldsymbol{P}_{k-1} \boldsymbol{A}_k^{\mathrm{T}} + \boldsymbol{Q}_k\right) \boldsymbol{H}_k^{\mathrm{T}}}{\boldsymbol{R}_k + \boldsymbol{H}_k \left(\boldsymbol{A}_k \boldsymbol{P}_{k-1} \boldsymbol{A}_k^{\mathrm{T}} + \boldsymbol{Q}_k\right) \boldsymbol{H}_k^{\mathrm{T}}}, \ \forall k \in \mathcal{K}, \tag{16}$$

where $\boldsymbol{P}_{k-1}$ is the error co-variance matrix at the last moment. Then, the real-time HC of customer i at the moment k can be given as follows:

$$\rho_{h,k}^i = \frac{\boldsymbol{z}_k \boldsymbol{H}_k(i) \cdot \hat{\boldsymbol{x}}_k(i)}{|\boldsymbol{z}_k|^2} \times 100\%, \ \forall i \in \mathcal{I}, \forall k \in \mathcal{K}, \forall h \in \mathcal{H}, \tag{17}$$

and the HC of the BH at the moment k can be given as follows:

$$\rho_{h,k}^{\mathrm{BH}} = \left(1 - \sum\nolimits_{i \in \mathcal{I}} \rho_{h,k}^i\right) \times 100\%, \ \forall k \in \mathcal{K}, \forall h \in \mathcal{H}. \tag{18}$$

With this two-stage estimator, the real-time HC of each customer can be evaluated with information at the current sampling moment, which is better than the data collection over a long period of time (e.g., numerous samples are needed in (2)). As shown in Fig. 3, compared with periodic evaluation methods, the lengthy data collection time can be avoided by the proposed real-time evaluation method. In addition, real-time HCs can be available immediately at the moment of measurement sampling so that the proposed method can capture the dynamic HCs of harmonic customers.

B. Dominant Index Method for Quantifying BH Fluctuations

Although the proposed two-stage estimator is capable of capturing the dynamic HCs of customers in real time, the

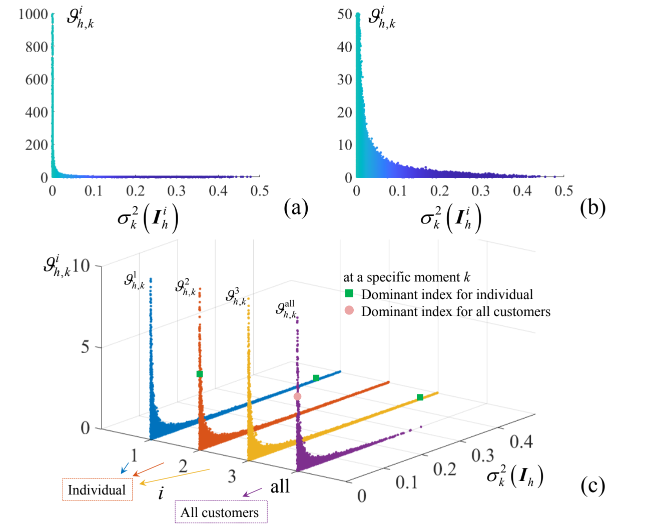

Fig. 4. The correlation between $\sigma_k^2(\boldsymbol{I}_h^i)$ and $\vartheta_{h,k}^i$ (a) individual; (b) enlarged graph of individual; (c) three individuals and all customers.

accuracy may be impacted by BH fluctuations. This is because the measurement data consists of two parts, i.e., customer harmonics and BH. The customer's HCs are difficult to evaluate accurately when BH is unstable. Moreover, the data with unstable BH is difficult to identify, since the information about BHs is always unknown and cannot be observed directly. To determine the negative effects on measurement data caused by BH fluctuations, the dominant index method is developed.

1) Dominant Index for Individual: First, a variance formulation at the moment k is defined to quantify the degree of fluctuation, which is shown as follows:

$$\sigma_k^2[X] = \frac{\sum_{k \in \mathcal{K}_\sigma} \left[X_k - 1/n \sum_{k \in \mathcal{K}_\sigma} X_k\right]^2}{n}, \tag{19}$$

where $\sigma_k^2[\ ]$ operator indicates the variance; X represents the variable; n is the sample number; $\mathcal{K}_\sigma$ is the set of samples for variance calculation, i.e., $\mathcal{K}_\sigma = \{[k-n+1, k] | k \in \mathbb{Z}\}$.

Equation (1) reveals that the harmonic at the PCC consists of two parts, namely the BH ($\boldsymbol{I}_h^{\mathrm{BH}}$) and customer harmonics ($\boldsymbol{I}_h^i$). In theory, the BH dominates the harmonic fluctuation at the PCC when the value of $\sigma_k^2[\boldsymbol{I}_h^{\mathrm{BH}}]/\sigma_k^2[\boldsymbol{I}_h^i]$ is large. On this basis, a dominant index is defined to reflect this relationship, which is shown as follows:

$$\vartheta_{h,k}^i = \sigma_k^2[\boldsymbol{I}_h^{\mathrm{BH}}]/\sigma_k^2[\boldsymbol{I}_h^i], \ \forall i \in \mathcal{I}, \forall k \in \mathcal{K}, \forall h \in \mathcal{H}, \tag{20}$$

where $\vartheta_{h,k}^i$ is the dominant index at the moment k. The information about BH (i.e., $\sigma_k^2[\boldsymbol{I}_h^{\mathrm{BH}}]$) is usually unavailable and the exact value of the variable $\vartheta_{h,k}^i$ is uncertain. However, this variable does not need to be calculated accurately. This is because whether BH is the dominant factor can be determined with the measured denominator $\sigma_k^2[\boldsymbol{I}_h^i]$. From the mathematical perspective, the ratio of two variables will tend to be zero with the increase of the absolute value of the denominator, since the ratio model is somehow like an inverse proportional function for the denominator variable. Therefore, with the increase of $\sigma_k^2[\boldsymbol{I}_h^i]$, the ratio $\vartheta_{h,k}^i$ will tend to zero. To illustrate this, a simple example is given here. $\sigma_k^2[\boldsymbol{I}_h^{\mathrm{BH}}]$ and $\sigma_k^2[\boldsymbol{I}_h^i]$ are positive numbers and supposed to follow the positive part of Gaussian distribution. The mathematical expectation and variance of them are set to be 0 and 0.1, respectively. The correlation between $\sigma_k^2(\boldsymbol{I}_h^i)$ and $\vartheta_{h,k}^i$ is shown in Fig. 4. As illustrated in Fig. 4 (a) and (b), the dominant index $\vartheta_{h,k}^i$ tends to zero with the increase of $\sigma_k^2[\boldsymbol{I}_h^i]$. To avoid misunderstandings, we additionally define another dominant index $\widetilde{\vartheta}_{h,k}^i$ from the statistical perspective, i.e., statistical dominant index (SDI), as follows:

$$\widetilde{\vartheta}_{h,k}^i = 1/\sigma_k^2[\boldsymbol{I}_h^i],\ \forall i \in \mathcal{I}, \forall k \in \mathcal{K}, \forall h \in \mathcal{H}. \tag{21}$$

Therefore, even without the information on BH $\sigma_k^2[\boldsymbol{I}_h^{\mathrm{BH}}]$, the dominant index $\vartheta_{h,k}^i$ can tend to zero statistically by choosing a large denominator $\sigma_k^2[\boldsymbol{I}_h^i]$, which means BH is not the dominant factor on the harmonic fluctuations at the PCC and has a limited impact on the accuracy of the real-time estimator.

By using the dominant index method, the severity of the BH fluctuation can be determined. However, the dominant index for an individual customer is not enough since multiple customers are considered in our problem. Hence, a dominant index for all customers is presented below.

2) Dominant Index for All Customers: The dominant index for all the customers $\vartheta_{h,k}^{\mathrm{all}}$ can be shown as:

$$\vartheta_{h,k}^{\mathrm{all}} = \sigma_k^2[\boldsymbol{I}_h^{\mathrm{BH}}]/\eta_{h,k},\ \forall i \in \mathcal{I}, \forall k \in \mathcal{K}, \forall h \in \mathcal{H}, \tag{22}$$

$$\eta_{h,k} = \min_{i \in \mathcal{I}} \sigma_k^2[\boldsymbol{I}_h^i],\ \forall k \in \mathcal{K}, \forall h \in \mathcal{H}, \tag{23}$$

where $\eta_{h,k}$ is the minimum value of $\sigma_k^2[\boldsymbol{I}_h^i]$ for $i \in \mathcal{I}$. If the minimum variance $\eta_{h,k}$ is still sufficiently large, all the variance for $i \in \mathcal{I}$ will also be large, which leads to the dominant index for all the customers $\vartheta_{h,k}^{\mathrm{all}}$ converging to zero. As a result, the impact of BH fluctuations is limited for all customers.

Fig. 4 (c) shows an example. The dominant index of measurement data for all considered moments in $\mathcal{K}$ are plotted as curves. At a specific moment k, the $\vartheta_{h,k}^{\mathrm{all}}$ is equal to the dominant index of the 2nd customer, since $\sigma_k^2[\boldsymbol{I}_h^2]$ is minimum compared to the variance of the 1st and 3rd customers. Then the dominant index curve for all the customers can be generated based on (22)-(23), as shown in the purple curve in Fig. 4 (c).

This curve can be used to determine the negative effect on measurement data caused by BH fluctuations. For example, if the $\vartheta_{h,k}^{\mathrm{all}}$ in the purple curve is close to zero at the moment k, the BH fluctuations will be limited. In other words, the credibility of the measurement data is high at the moment k.

C. Adaptive Gain Selection Strategy for Improving Evaluation Accuracy

From the above analysis, we know that when the dominant index $\vartheta_{h,k}^{\mathrm{all}}$ is large, the credibility of the measurement data is not high due to the negative effects of BH fluctuations, and the error of the measurement model is also large. This error makes the two-stage iteration estimator inaccurate, which can damage the performance of the real-time HC evaluation. Therefore, the parameter $\boldsymbol{R}_k$ of the measurement model in (5) and (9) should be designed properly to match the negative effects caused by BH fluctuations. To this end, an adaptive gain selection strategy is proposed to mitigate the negative effects and improve the accuracy of real-time HC evaluation even under conditions with BH fluctuations.

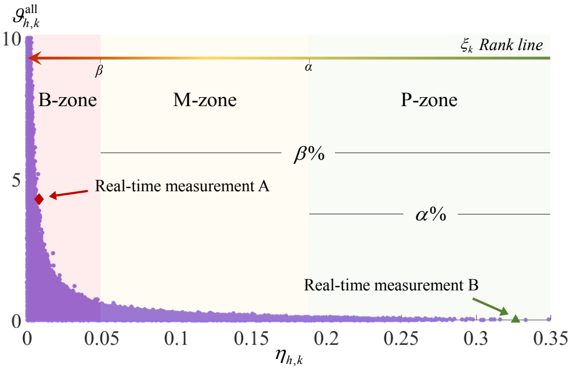

Fig. 5. Ranking zones for real-time measurement data.

The key to this strategy is that when the measurement model error is large, we weaken the inappropriate measurement correction by tuning the error and gain parameters. Conversely, when the measurement model error is small, we reinforce the changes made by the measurement correction, since it can improve the accuracy of the evaluation. On this basis, the correction gain in (16) can be modified as follows:

$$\boldsymbol{G}_k = \frac{\left(\boldsymbol{A}_k \boldsymbol{P}_{k-1} \boldsymbol{A}_k^{\mathrm{T}} + \boldsymbol{Q}_k\right) \boldsymbol{H}_k^{\mathrm{T}}}{\boldsymbol{R}_k^{\mathrm{adpt}} + \boldsymbol{H}_k \left(\boldsymbol{A}_k \boldsymbol{P}_{k-1} \boldsymbol{A}_k^{\mathrm{T}} + \boldsymbol{Q}_k\right) \boldsymbol{H}_k^{\mathrm{T}}},\ \forall k \in \mathcal{K}, \tag{24}$$

where $\boldsymbol{R}_k^{\mathrm{adpt}}$ is the adaptive error co-variance matrix and can be expressed as:

$$\boldsymbol{R}_k^{\mathrm{adpt}} = \gamma_k \boldsymbol{E},\ \forall k \in \mathcal{K}, \tag{25}$$

where $\boldsymbol{E}$ is the identity matrix; γ_k is a weight function and can be expressed as:

$$\gamma_k = \begin{cases} 0, & \xi_k \in \text{P-zone} \\ \frac{\alpha\beta(\epsilon - \Psi - \eta_k) + \Psi \eta_k}{(\beta - \alpha)\eta_k}, & \xi_k \in \text{M-zone} \\ \Psi, & \xi_k \in \text{B-zone} \end{cases},\ \forall k \in \mathcal{K}, \tag{26}$$

$$\xi_k = rank[\eta_k],\ \forall k \in \mathcal{K}, \tag{27}$$

where Ψ is a parameter of the weight function, which is a large enough number; $rank[\ ]$ is the function used to rank the η_k at different moments; ξ_k is the ranking result for determining the severity caused by BH fluctuations on the measurement data, which is illustrated in detail in Fig. 5. It is noted that Fig. 5 is the dominant index for all customers in Fig. 4 (c). It can be seen that there are three zones referring to the horizontal axis, i.e., P-zone, M-zone, and B-zone. Upper and lower thresholds are set to α and β, respectively. Measurement data with $\alpha\%$ (e.g., 50%) highest ranking in P-zone are considered high-quality data, and below $\beta\%$ (e.g., 80%) in B-zone are bad data. The M-zone is with intermediate data, where the dominant index increases with the ranking decrease. There are two examples, i.e., measurements A and B. The real-time measurement data A is ranked in B-zone (the red one), which means the dominant index is large. In contrast, the real-time measurement data B is ranked in P-zone (the green

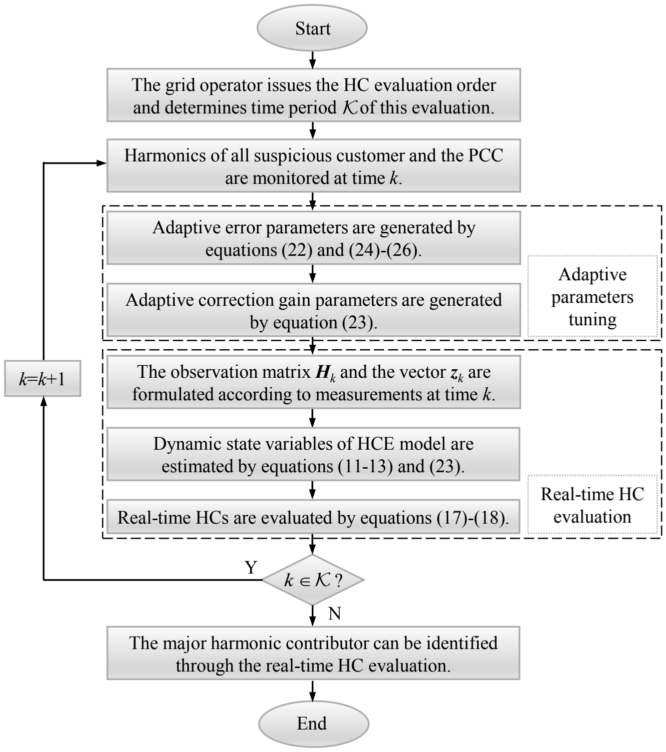

Fig. 6. The procedure of real-time HC evaluation method.

one), which means the dominant index is small, and the effect caused by BH fluctuations can be trivial. By outputs of weight function γ_k in (26), the correction gain $\boldsymbol{G}_k$ in (24) can be tuned properly to improve the accuracy of real-time HC evaluation.

In order to elaborate on the application way in practice, the implementation procedure of the proposed real-time HC evaluation method is illustrated in Fig. 6.

IV. Numerical Studies

To verify the proposed real-time HC evaluation method, the revised IEEE test system for harmonics modeling and simulation is established by utilizing PSCAD/EMTDC. This test system is a distribution network, as shown in Fig. 7. Both bus 1 (slack bus at 69 kV) and bus 4 (13.8 kV) are connected to power supplies, and this distribution network is fed from them. The simulation data is performed based on the '*Test System for Harmonics Modeling and Simulation*', which is provided and published by the IEEE Power Engineering Society (IEEE PES) [34]. More details about the IEEE test system refer to [34]. Customers on buses 7, 10, and 13 are considered harmonic producers. These customers' harmonic emission characteristics and rated power are illustrated in Table I, which are scaled based on the fundamental currents. The time interval of HC evaluation is 12 hours (8 a.m.-8 p.m.). To show the variability of customer behavior, we assume that customers 10 and 13 are connected to the distribution network only during working hours (9-12 a.m., 2-5 p.m.) and some short periods of time (10-12 a.m., 3-4 p.m., 6-7 p.m.), respectively. Intuitively, the sequence of connecting hours is shown in Table II. All of them have 30% standard normal random fluctuations. The PCC is bus 3, where power quality is checked, and the harmonic

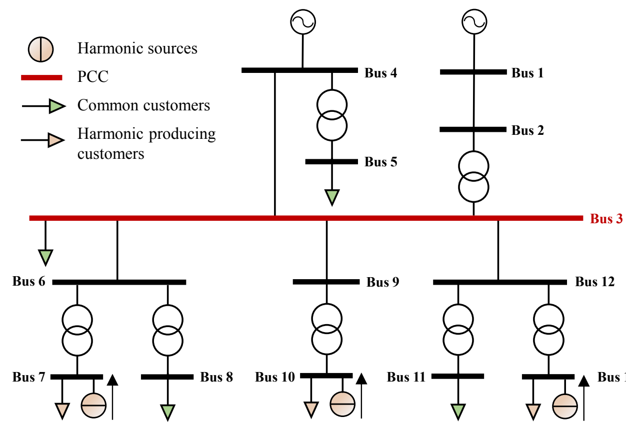

Fig. 7. IEEE test system No.3 for harmonic modeling and simulation.

TABLE I
Harmonic Emission Spectrum and Rated Power

Harmonic Order	Customer 7	Customer 10	Customer 13
	Magnitude (percent) / Relative Angle (degree)		
1-st	100 / 0	100 / 0	100 / 0
5-th	15.6 / -42.06	28.37 / -37.19	– / –
7-th	11.66 / -48.65	22.54 / -46.13	– / –
11-th	6.87 / -55.81	– / –	13.74 / -54.26
13-th	5.80 / -58.22	– / –	11.84 / -58.39
Power (kW/kvar)	1150 / 290	810 / 800	2850 / 2500

monitors are performed on all suspicious customers and the PCC. In our study, the measurement sampling period is fifteen minutes. The proposed real-time HC evaluation method is verified in four different cases, as below.

A. Verification Without Background Harmonic Fluctuations

In the first case, the HCs of these customers are evaluated by the proposed method without considering BH fluctuations. To validate the performance of our method, HCs are also evaluated by two periodic methods, i.e., the CLSR method and the data selection method. Fig. 8 shows the evaluation results by different methods. The 'exactness' represents actual results derived based on invasive measurement and superposition theory. Note that even though the invasive scheme is harmful to the distribution network, it is appropriate to be used for numerical verification due to its accuracy. Moreover, to describe the accuracy in detail, the errors of evaluation are shown in Table III, which are scaled based on the exactness value.

According to Fig 8, the evaluation results show that the 11-th and 13-th harmonics are rarely contributed by customer 10. The 5-th and 7-th harmonics at the PCC are rarely contributed

TABLE II
Working Time of Harmonic Producing Customers

Time (h) Sequence	1	2	3	4	5	6	7	8	9	10	11	12
Customer 7	Y	Y	Y	Y	Y	Y	Y	Y	Y	Y	Y	Y
Customer 10	-	Y	Y	Y	-	-	Y	Y	Y	-	-	-
Customer 13	-	-	Y	Y	-	-	-	Y	-	-	Y	-

TABLE III
ERRORS OF EVALUATION BY DIFFERENT METHODS

Method	CLSR Method					Data Selection Method					Proposed Method				
Harmonic Order	Main grid	Customer			TE	Main grid	Customer			TE	Main grid	Customer			TE
		7	10	13			7	10	13			7	10	13	
5-th	5.79%	1.88%	2.23%	0.19%	10.09%	5.36%	0.72%	4.00%	0.21%	10.29%	1.09%	0.67%	0.42%	0.00%	2.18%
7-th	5.68%	5.44%	0.27%	0.03%	11.41%	5.51%	2.17%	3.33%	0.02%	11.02%	1.21%	1.15%	0.07%	0.00%	2.43%
11-th	3.03%	5.56%	0.06%	2.59%	11.24%	2.64%	5.19%	0.07%	2.62%	10.52%	1.18%	1.22%	0.00%	0.04%	2.44%
13-th	4.06%	5.75%	0.05%	1.64%	11.50%	4.76%	5.25%	0.09%	0.39%	10.49%	1.11%	1.21%	0.00%	0.11%	2.43%

TABLE IV
TES OF EVALUATION BY DIFFERENT METHODS UNDER BH FLUCTUATIONS

BH	CLSR Method				Data Selection Method				Proposed Method			
Fluctuations	5-th	7-th	11-th	13-th	5-th	7-th	11-th	13-th	5-th	7-th	11-th	13-th
10%	14.83%	14.54%	14.28%	14.29%	12.07%	12.76%	12.73%	12.16%	2.79%	2.87%	2.99%	2.91%
20%	18.43%	18.39%	17.66%	17.38%	12.68%	13.46%	13.63%	13.38%	3.27%	3.06%	3.28%	3.39%
30%	26.87%	25.03%	22.33%	25.86%	14.56%	14.83%	14.76%	14.35%	4.54%	4.18%	4.47%	4.16%

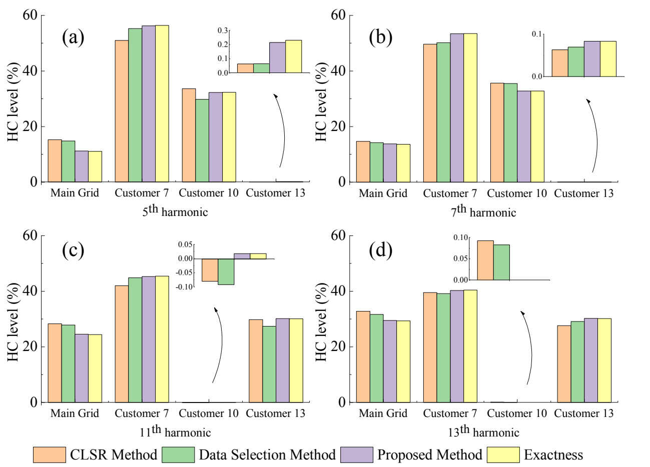

Fig. 8. HC evaluation results based on different methods (a) 5-th harmonic; (b) 7-th harmonic; (c) 11-th harmonic; (d) 13-th harmonic.

by customer 13. These conclusions are matched with reality, as shown in Table I, which indicates the proposed method is effective. Moreover, from Fig 8, we can observe that the proposed method is more accurate than the two other periodic methods. This observation is further illustrated in Table III. The total error (TE) for the h-th harmonic is the sum of evaluation errors of the h-th harmonic for the BH and all customers, which can be shown as follows:

$$\mathrm{TE}_h = \sum_{i\in\mathcal{I},k\in\mathcal{K}} \mathcal{E}\left[\rho_{h,k}^{i}\right] + \mathcal{E}\left[\rho_{h,k}^{\mathrm{BH}}\right],\ \forall h \in \mathcal{H}, \tag{28}$$

where TE_h is the total HC evaluation error for the h-th harmonic; $\mathcal{E}[\,]$ operator represents the error of HC estimation.

The TEs of two periodic methods (i.e., the CLSR and data selection methods) are more than 10% for any harmonic order, while the TE of the proposed method is within 2.5%. These results are reasonable because customer behaviors change several times within the periodic time interval, but periodic methods cannot capture these dynamic changes. By contrast, the proposed method can track the time-varying harmonic characteristic in time. Therefore, the HCs can be evaluated more accurately by the proposed method.

B. Verification With Background Harmonic Fluctuations

In the second case, to verify the robustness of the proposed method under BH fluctuations, different BH fluctuations are considered, i.e., 10%, 20%, and 30% standard normal random fluctuations. The TEs of evaluation by different methods under the impact of BH fluctuations are expressed in Table IV.

It can be found from Table IV that for different methods, TEs of any harmonic orders become larger with BH fluctuations increasing. The TEs of the proposed method are always small than the TEs of two other periodic methods under different BH fluctuations. When the BH fluctuations reach up to 30%, all the TEs of the CLSR method and the data selection method are around 25% and 14%, respectively, while the TEs of the proposed method are three times lower than the TEs of two other methods (only about 4.5%). This is because the error co-variance matrix $\boldsymbol{R}$ and the correction gain matrix $\boldsymbol{G}$ can be self-tuned according to the severity of BH fluctuations and the negative effect on the proposed iteration estimator is weakened. Therefore, the evaluation can be more accurate even under conditions with BH fluctuations.

In this case, real-time HC evaluations are demonstrated based on the proposed method. Taking the 5-th harmonic as an example, the dynamic changes of HCs can be described in real time, as shown in Fig. 9.

C. Verification of Real-time Evaluation

In order to reflect the superiority of real-time evaluation intuitively, the comparison of evaluations under different scales of time is illustrated, as shown in Fig. 10. The evaluation with the overall process in Fig. 10 (a) represents the general contribution of the main grid and customers during half of a day, while the evaluations with hourly time-scales in Fig. 10 (b) characterize more details about dynamic changes of HC level.

According to periodic methods, the HC percentage of customer 7 is about 55%, which is higher than that of the

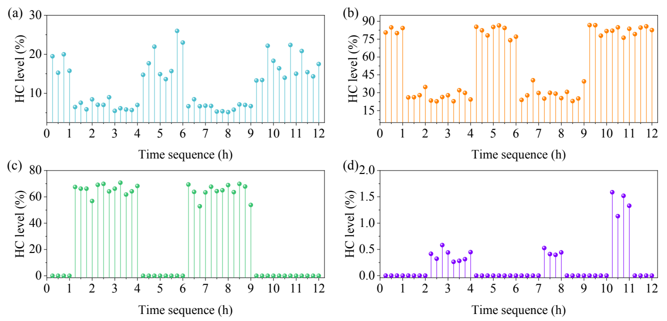

Fig. 9. Real-time evaluation results of 5-th harmonic for the main grid and customers (a) main grid; (b) customer 7; (c) customer 10; (d) customer 13.

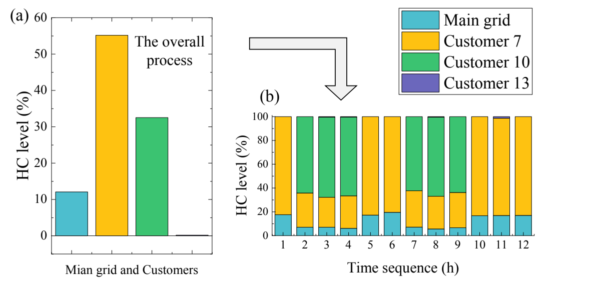

Fig. 10. Comparison of evaluations under different time-scales for 5-th harmonic (a) the overall process (half of a day); (b) hourly.

main grid and other customers. Based on this information from the overall process, the most serious harmonic contributor is customer 7. However, we have new discoveries by observation based on the real-time evaluation. According to the real-time evaluation in Fig. 9, the HC of customer 7 is more than 80% in the first hour. However, it decreases dramatically in the second hour due to the connection of customer 10. Moreover, at this time, the HC level of customer 10 is about 60%-70%, which is higher than that of customer 7. That means if customer 10 connects to the distribution network, it will become the major harmonic contributor for the 5-th harmonic. More dynamic information can be provided in detail based on the proposed real-time evaluation method. As a result, the major harmonic contributor can be identified in real time.

To verify this advantage of the real-time evaluation, another comparison of evaluations under different time-scale is also developed for the 11-th harmonic. The dynamic changes of HCs for 11-th harmonic can also be described in real time, as shown in Fig. 11. Results under half of a day and hourly time-scales are shown in Fig. 12 (a) and (b), respectively. According to Fig. 12(a), the HC level of customer 7 is higher than 45% under the overall process time-scale. Besides, as shown in Fig. 12(b), customer 7 is always contributing 11-th harmonics during half of a day scale of time. That is the reason why the cumulative harmonic contribution of customer 7 is more than that of other customers. However, the actual major harmonic contributor for the 11-th harmonic is customer 13. That is because, from the results of the real-time evaluation in Fig. 12 (b), we can observe that customer 13 will contribute the most harmonics (about 90%) and become the major harmonic contributor if customer 13 connects to the distribution network.

In addition, the analytical plots for the 7-th harmonic and the 13-th harmonic are also given here as Fig. 13. From Fig. 13 (b), it can be seen that if customer 10 is connected

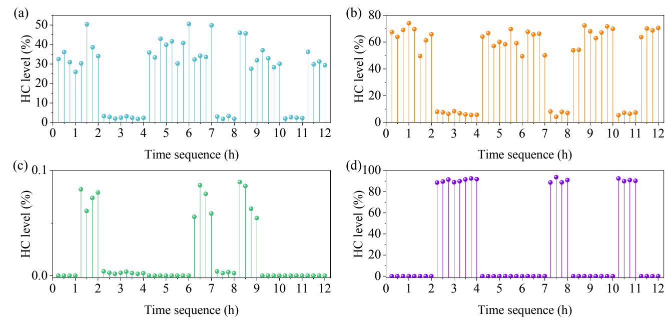

Fig. 11. Real-time evaluation results of 11-th harmonic for the main grid and customers (a) main grid; (b) customer 7; (c) customer 10; (d) customer 13.

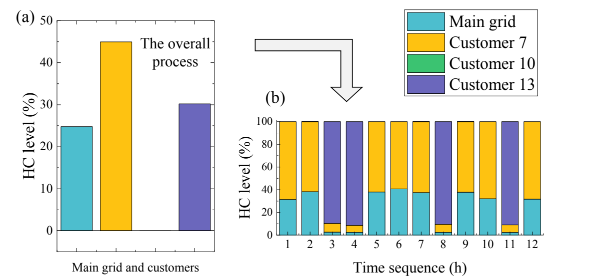

Fig. 12. Comparison of evaluations under different time-scales for 11-th harmonic (a) the overall process (half of a day); (b) hourly.

to the distribution network, the HC level of customer 10 will be more than 60%. Therefore, customer 10 is the major harmonic contributor for the 7-th harmonic. Moreover, from the evaluation under half of a day time-scale in Fig. 13 (c), the HC percentage of customer 7 is around 37%, which is higher than that of the main grid and other customers. However, according to evaluation under the hourly time-scale in Fig. 13 (d), if customer 13 is connected to the distribution network, the HC level of customer 13 will be around 90%. Therefore, customer 13 is the major harmonic contributor for the 13-th harmonic.

In conclusion, dynamic harmonic characteristics are lost in evaluation results by the original rough scale (e.g., Fig. 12(a)). Benefiting from our proposed method (e.g., Fig. 12(b)), the

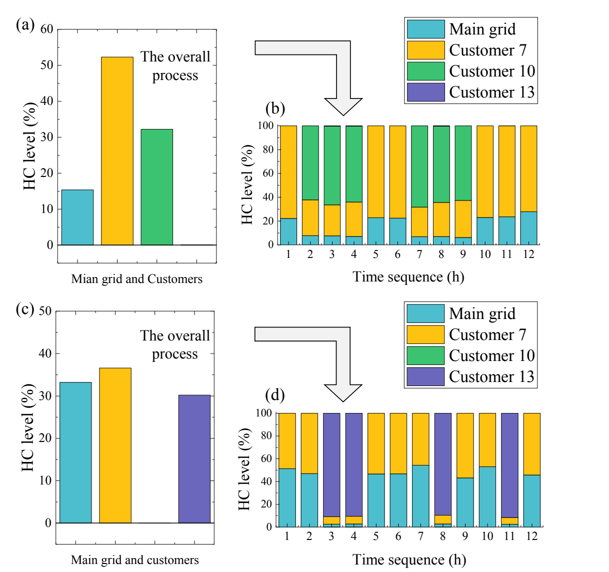

Fig. 13. Comparison of evaluations under different time-scales for 7-th harmonic (a) the overall process (half of a day); (b) hourly; and 13-th harmonic (c) the overall process (half of a day); (d) hourly.

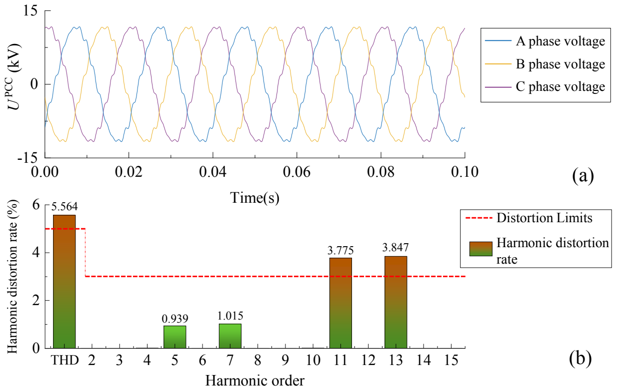

Fig. 14. The voltage at the PCC before harmonic suppression (a) time-domain three-phase waveform; (b) frequency-domain harmonic distortion rate.

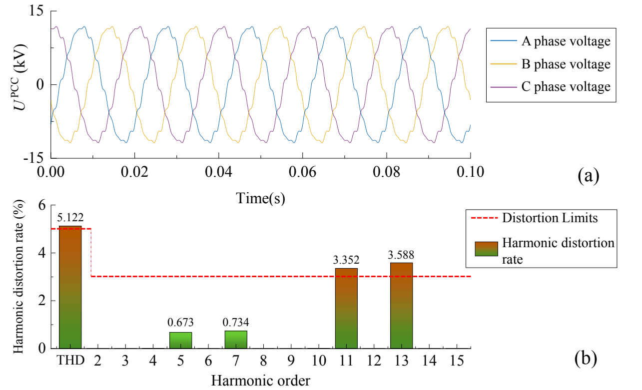

Fig. 15. The voltage at the PCC under the first suppression scheme based on periodic methods (a) time-domain three-phase waveform; (b) frequency-domain harmonic distortion rate.

changes in HC levels can be discovered in real time. Furthermore, the actual major harmonic contributor can be identified from this dynamic description based on our proposed method.

D. Example Application of Harmonic Suppression Based on the Proposed Method

To demonstrate the significance of the proposed method in practice, the effects of harmonic suppression based on different methods are compared in this case. Taking 11:00 a.m. as an example, the original voltage at the PCC is shown in Fig. 14. According to Fig. 14 (a), the three-phase voltage waveform at the PCC has obvious harmonic distortion. Moreover, the voltage spectrum in Fig. 14 (b) shows that the 11-th and 13-th individual harmonic distortions (IHDs) and total harmonic distortion (THD) exceed the distortion limits [35]. Therefore, harmonic suppression measures should be implemented to improve the power quality at the PCC.

To suppress the harmonic distortion at the PCC, the harmonic suppression device should be set at the bus where the major harmonic contributor is located. There are two harmonic suppression schemes in this case. The first one is based on the CLSR and data selection methods. As the results of these two periodic methods, the major contributor for any harmonic orders is always customer 7. Hence, for the first scheme, the harmonic suppression device should be set for customer 7. The voltage at the PCC after the first harmonic suppression scheme is shown in Fig. 15. It shows that the distortion of the time-domain voltage waveform is improved slightly. According to Fig. 15 (b), we can observe that although all the IHDs and THD are decreased, the IHDs (11-th, 13-th) and THD still exceed the distortion limit. These results show that the first scheme, which is based on periodic methods under a large scale of time, has very limited effectiveness.

The second harmonic suppression scheme is based on our proposed method. As the real-time evaluation result shown in Fig. 9, the actual major contributor to 5-th harmonic is customer 10. From Fig. 12, the major contributor to 11-th harmonic is customer 13. The HC levels for 7-th and 13-th are similar to the 5-th and 11-th harmonics, respectively. Thus, in the second scheme, harmonic suppression devices for 5-th and 7-th harmonics are set for customer 10. The 11-th and 13-th harmonic suppression devices are set for customer 13. The

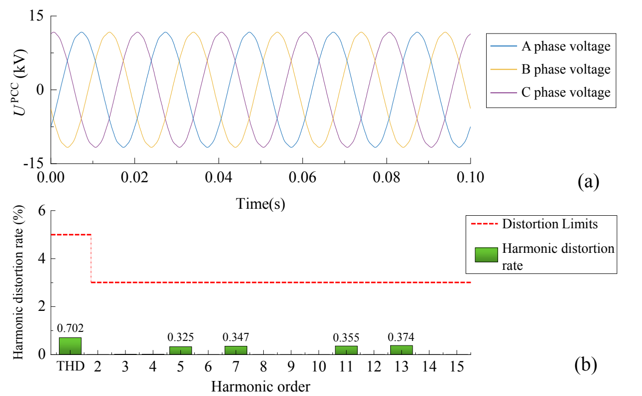

Fig. 16. The voltage at the PCC under the second suppression scheme based on the proposed method (a) time-domain three-phase waveform; (b) frequency-domain harmonic distortion rate.

harmonic suppression effect by the second scheme is shown in Fig. 16, where the voltage waveform in the time-domain is improved dramatically and becomes very smooth. All the IHDs and THD in the frequency-domain are well below the distortion limit [35]. That is because the dynamic HC level is captured in real time by using the proposed method. On this basis, the actual major harmonic contributor can be identified accurately. Therefore, the second suppression scheme based on our proposed method is effective.

Without loss of generality, another case at 2:00 p.m. is given to demonstrate the difference between the two algorithms. The frequency-domain harmonic distortion rate of the voltage (i) before harmonic suppression, (ii) under the first suppression scheme based on periodic methods, and (iii) under the second suppression scheme based on the proposed method are shown as the following Table V.

From Table V, it can be seen that after different harmonic suppression schemes, the distortion of voltage is improved. However, based on the proposed method, the THD is around 0.568%, which is significantly lower than the 1.058% based on the first scheme. Moreover, based on the proposed method, the 5-th and 7-th IHDs are around 0.334% and 0.356%, respectively, which are also remarkably lower than the 0.681% and 0.756% based on the first scheme. These remarkable harmonic suppression results show the second scheme based on our proposed method is very effective and further demonstrates

TABLE V
FREQUENCY-DOMAIN HARMONIC DISTORTION RATE UNDER DIFFERENT SITUATIONS

Different situations	Harmonic distortion rate				
	THD	5-th	7-th	11-th	13-th
Before suppression	1.518%	0.957%	1.042%	0.366%	0.383%
First suppression scheme	1.058%	0.681%	0.756%	0.189%	0.222%
Second suppression scheme	0.568%	0.334%	0.356%	0.189%	0.221%

TABLE VI
PER-UNIT LINE AND CABLE IMPEDANCE DATA
(BASED VALUES: 13.8KV, 10000KVA)

From	To	R	X
Bus 1	Bus 2	0.00139	0.00296
Bus 3	Bus 4	0.00122	0.00243
Bus 3	Bus 6	0.00075	0.00063
Bus 3	Bus 9	0.00157	0.00131
Bus 3	Bus 12	0.00109	0.00091

the superiority of the proposed real-time evaluation method.

V. CONCLUSION

To accommodate the dynamic harmonic characteristic of customers, a real-time HC evaluation method is proposed for the first time. Specifically, this method is established by a two-stage iteration estimator based on the information fusion idea to quantify the dynamic HCs of each customer in real time. By using the proposed method, the time-varying HCs can be evaluated since each customer's HCs can be available immediately at the moment of measurement sampling. On this basis, the actual major harmonic contributor can be identified, and the THD of voltage at the PCC can be suppressed from 5.564% to 0.702%, which is well below the distortion limit of the IEEE standard. Furthermore, a dominant index method is developed to determine the negative effect of BH fluctuations, and then an adaptive gain selection strategy is proposed to improve the evaluation accuracy with BH fluctuations. Compared to periodic methods, the errors for any harmonic order are reduced from about 10% to within 2.5%. The TEs of the proposed method can remain around only 4.5% even under the condition with 30% BH fluctuations. The proposed method contributes to the power quality management of distribution networks.

Harmonic instability problems may occur in the distribution network, which can degrade the power quality and make identifying the major harmonic contributor more challenging. This issue still needs to be addressed. Therefore, the authors will consider the harmonic instability phenomenon in the research of harmonic contribution evaluation in future work.

APPENDIX A: SOURCE OF SIMULATION DATA

Some important simulation data are given in this part. The per-unit line and cable impedance data, transformer data, and generation and load data are shown in Tables VI, VII, and VIII, respectively.

TABLE VII
TRANSFORMER DATA

From	To	Voltage(kV)	kVA	%R	%X
Bus 2	Bus 1	69:13.8	15000	0.4698	7.9862
Bus 4	Bus 5	13.8:0.48	1500	0.9593	5.6694
Bus 6	Bus 7	13.8:0.48	1250	0.7398	4.4388
Bus 6	Bus 8	13.8:0.48	1725	0.7442	5.9537
Bus 9	Bus 10	13.8:0.48	1500	0.8743	5.6831
Bus 12	Bus 11	13.8:0.48	1500	0.8363	5.4360
Bus 12	Bus 13	13.8:2.4	3750	0.4568	5.4810

TABLE VIII
GENERATION AND LOAD DATA

Bus	P_{gen}(kW)	Q_{gen}(kvar)	P_{load}(kW)	Q_{load}(kvar)
Bus 1	7450	540	–	–
Bus 3	–	–	2240	2000
Bus 4	2000	1910	–	–
Bus 5	–	–	600	530
Bus 7	–	–	1150	290
Bus 8	–	–	1500	0.8363
Bus 10	–	–	810	800
Bus 11	–	–	370	330
Bus 13	–	–	2800	2500

APPENDIX B: A COMPARISON OF SEVERAL METHODS IN ANOTHER CASE

In order to make the experimental conclusions more convincing, another case is given to compare these several estimation methods. In this case, the time interval of evaluation is 6 hours, which is different. Customer 7 is connected to the grid throughout the evaluation's time interval. However, customer 10 and customer 13 are connected to the grid for one hour in the fourth hour. The errors of harmonic contribution evaluation by two periodic methods and our proposed real-time method are shown in Table IX.

From Table IX, it can be seen that the TEs of the CLSR method and data selection method are more than 12% and 10% for any harmonic order, respectively. However, the TE of the proposed method is within 2.5%, which is significantly lower than that of the other two periodic methods. Therefore, the proposed evaluation method is more accurate. This is reasonable since information on the HCs at each sampling moment can be available through the real-time evaluation of the proposed method.

APPENDIX C: DISCUSSION ON TRANSFORMER PARAMETERS

For a specific transformer, changes in parameters have different impacts on customers in different locations.

TABLE IX
ERRORS OF EVALUATION BY DIFFERENT METHODS

Method	CLSR Method					Data Selection Method					Proposed Method				
Harmonic Order	Main grid	Customer 7	Customer 10	Customer 13	TE	Main grid	Customer 7	Customer 10	Customer 13	TE	Main grid	Customer 7	Customer 10	Customer 13	TE
5-th	5.14%	4.89%	2.02%	0.03%	12.08%	5.42%	3.34%	2.03%	0.05%	10.84%	0.53%	1.03%	0.50%	0.00%	2.06%
7-th	5.78%	6.36%	0.56%	0.02%	12.72%	4.15%	5.56%	1.40%	0.01%	11.12%	1.06%	0.57%	0.50%	0.00%	2.13%
11-th	5.11%	6.02%	0.19%	1.10%	12.42%	5.47%	4.54%	0.01%	0.94%	10.96%	1.12%	1.20%	0.00%	0.07%	2.39%
13-th	4.92%	6.21%	0.01%	1.30%	12.44%	5.70%	3.54%	0.10%	2.06%	11.40%	0.86%	1.03%	0.00%	0.18%	2.07%

TABLE X
HC PERCENTAGE OF 5-TH HARMONIC FOR CUSTOMERS AT DIFFERENT LOCATIONS

Scenarios	Transformer parameters	Main Grid	Customer 7	Customer 10	Customer 13
Scenario 1	%R = 0.2	5.3836%	15.5896%	78.8055%	0.2213%
Scenario 2	%R = 0.3	5.3895%	17.9182%	76.4333%	0.2590%
Scenario 3	%R = 0.6	5.4145%	24.0205%	70.2073%	0.3577%

- If the parameters of the transformer in a specific feeder are changed, the harmonic of the customer in this specific feeder will be affected, and the percentage of harmonic contribution of this feeder will also be affected.
- If the parameters of the transformer in a specific feeder are changed, the impact on the harmonic of customers in other feeders can be negligible. The percentage of harmonic contribution of other feeders will change relatively with the percentage changing of that specific feeder.

A comparison case is given to verify the effect of different transformer parameters. In this case, all the customers are connected to the distribution network. There are three scenarios set in this supplemented case. In different scenarios, the leakage reactance parameter of the transformer between customer 10 and the PCC is %R = 0.2, %R = 0.3, and %R = 0.6, respectively.

Take the 5-th harmonic as an example. The percentage of harmonic contribution of different customers in these three scenarios can be shown in Table X.

From Table X, it can be seen that with the increase of transformer impedance parameters (between customer 10 and the PCC), the percentage of harmonic contribution from customer 10 decreases (located at this feeder). However, the percentage of harmonic contribution from other customers increases relatively with the percentage decrease of customer 10 (located at other feeders).

This indicates that if the parameters of the transformer in a specific feeder are changed, the percentage of harmonic contribution of this feeder will be affected. Furthermore, the percentage of harmonic contribution of other feeders will change relatively with the percentage changing of that specific feeder.

APPENDIX D: DISCUSSION ON HARMONIC AMPLIFICATION

The harmonic amplification phenomenon is an undesired increase in the magnitude of harmonics, which can occur in two types of situations.

- The power capacitors added to the network may cause harmonic amplification. This is because the addition of capacitors leads to a reduction of system impedance. Capacitive impedance is inversely proportional to frequency; therefore, power capacitors have a lower impedance for high frequencies (e.g., 250Hz, 350Hz, 550Hz, and 650Hz). This leads to an increase in the magnitude of harmonic, i.e., harmonic amplification.
- The occurrence of harmonic resonances may also cause high magnification of harmonics. In a system with inductive impedance (X_{L}) and capacitive impedance (X_{C}), the harmonic resonance may occur at a specific frequency (resonant frequency, F_{R}). At this resonance point, X_{L} is equal to X_{C} and the impedance is very low; therefore, only inherent resistance in the network would limit the harmonic, and the magnitude of the harmonic (with frequency F_{R}) will be amplified.

A case about harmonic amplification is given. There are two scenarios in this case. (a) The first is a normal scenario, i.e., no harmonic amplification phenomenon. (b) In the second scenario, a power capacitor (9980 μF) is added to the PCC, which may result in harmonic amplification.

The frequency-domain harmonic distortion rate of voltage at the PCC under normal scenario and harmonic amplification scenario can be illustrated as following Figure 17 (a) and (b), respectively.

From the Figure 17, it can be seen that the 5-th, 7-th, 11-th, 13-th IHDs and the THD in the normal scenario are 0.938%, 1.015%, 3.775%, 3.847%, and 5.564%, respectively. However, in harmonic amplification scenario, the 5-th, 7-th, 11-th, 13-th IHDs and the THD are 1.198%, 1.543%, 31.351%, 12.778%, and 33.912%, respectively. The IHDs and the THD are amplified severely, which indicates that the harmonic amplification phenomenon occurs in the second scenario. Among the different harmonic orders, the harmonic amplification of the 11-th IHD is the most significant, with an amplification of about 8.3 times.

Taking the 11-th harmonic as an example, the HC for different customers before and after the occurrence of harmonic amplification are shown in Table XI.

From Table XI, the HC for the main grid, customer 7, cus-

TABLE XI
HC PERCENTAGE OF 11-TH HARMONIC FOR CUSTOMERS UNDER DIFFERENT SCENARIOS

Scenarios	Harmonic amplification	Main Grid	Customer 7	Customer 10	Customer 13
Scenario 1	No	2.1487%	6.7715%	0.0058%	90.9640%
Scenario 2	Yes	2.2482%	6.8667%	0.0026%	90.8825%

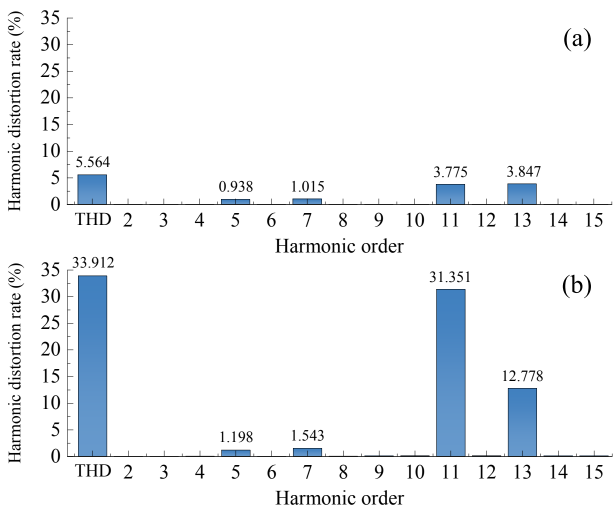

Fig. 17. The frequency-domain harmonic distortion rate of voltage at the PCC (a) normal scenario; (b) harmonic amplification scenario.

tomer 10, and customer 13 are 2.1487%, 6.7715%, 0.0058%, and 90.9640% in scenario 1 (normal scenario), respectively. In the harmonic amplification scenario, the HC for the main grid, customer 7, customer 10, and customer 13 are 2.2482%, 6.8667%, 0.0026%, and 90.8825%, respectively.

The results indicate that customer 13 is still the major contributor to the 11-th harmonic, regardless of the occurrence of harmonic amplification phenomenon. It is reasonable since the harmonic amplification phenomenon is caused by the added capacitor instead of other customers. Therefore, the multi-customers' HC can be evaluated, and major harmonic contributor can be identified with or without considering harmonic amplification.

REFERENCES

[1] H. Hua, Y. Qin, Z. He, L. Li, and J. Cao, "Energy sharing and frequency regulation in energy network via mixed H_2/H_∞ control with markovian jump," *CSEE Journal of Power and Energy Systems*, vol. 7, no. 6, pp. 1302–1311, 2020.

[2] P. Wang, Z. Zhang, T. Ma, Q. Huang, and W.-J. Lee, "Parameter calibration of wind farm with error tracing technique and correlated parameter identification," *IEEE Transactions on Power Systems*, Early Access, 2022.

[3] H. Hui, Y. Ding, K. Luan, T. Chen, Y. Song, and S. Rahman, "Coupon-based demand response for consumers facing flat-rate retail pricing," *CSEE Journal of Power and Energy Systems*, Early Access, 2022.

[4] Y. Chen, K.-W. Lao, D. Qi, H. Hui, S. Yang, Y. Yan, and Y. Zheng, "Distributed self-triggered control for frequency restoration and active power sharing in islanded microgrids," *IEEE Transactions on Industrial Informatics*, Early Access, 2023.

[5] H. Hua, J. Cao, G. Yang, and G. Ren, "Voltage control for uncertain stochastic nonlinear system with application to energy internet: Non-fragile robust H_∞ approach," *Journal of Mathematical Analysis and Applications*, vol. 463, no. 1, pp. 93–110, 2018.

[6] Y. Terriche, A. Laib, A. Lashab, C.-L. Su, J. M. Guerrero, and J. C. Vasquez, "A frequency independent technique to estimate harmonics and interharmonics in shipboard microgrids," *IEEE Transactions on Smart Grid*, vol. 13, no. 2, pp. 888–899, 2022.

[7] I. Papič, D. Matvoz, A. Špelko, W. Xu, Y. Wang, D. Mueller, C. Miller, P. F. Ribeiro, R. Langella, and A. Testa, "A benchmark test system to evaluate methods of harmonic contribution determination," *IEEE Transactions on Power Delivery*, vol. 34, no. 1, pp. 23–31, 2019.

[8] Y. Zhang, C. Lin, Z. Shao, and B. Liu, "A non-intrusive identification method of harmonic source loads for industrial users," *IEEE Transactions on Power Delivery*, vol. 37, no. 5, pp. 4358–4369, 2022.

[9] R. A. S. Fernandes, M. Oleskovicz, and I. N. da Silva, "Harmonic source location and identification in radial distribution feeders: An approach based on particle swarm optimization algorithm," *IEEE Transactions on Industrial Informatics*, vol. 18, no. 5, pp. 3171–3179, 2022.

[10] J. Cheng, Z. Yan, X. Xu, H. Wang, Y. Zhang, and S. Zhang, "A bivariate stochastic optimization model of bidding strategy considering the competition among renewable power producers," *CSEE Journal of Power and Energy Systems*, pp. 1–11, 2021.

[11] J.-A. Jiang, J.-C. Wang, H.-S. Wu, C.-H. Lee, C.-Y. Chou, L.-C. Wu, and Y.-C. Yang, "A novel sensor placement strategy for an IoT-based power grid monitoring system," *IEEE Internet of Things Journal*, vol. 7, no. 8, pp. 7773–7782, 2020.

[12] F. Safargholi, K. Malekian, and W. Schufft, "Voltage-current ratio difference" concept for identifying the dominant harmonic source," *International Journal of Electrical Power & Energy Systems*, vol. 121, p. 106147, 2020.

[13] M. Nagpal, W. Xu, and J. Sawada, "Harmonic impedance measurement using three-phase transients," *IEEE Transactions on Power Delivery*, vol. 13, no. 1, pp. 272–277, 1998.

[14] W. Xu, E. E. Ahmed, X. Zhang, and X. Liu, "Measurement of network harmonic impedances: practical implementation issues and their solutions," *IEEE Transactions on Power Delivery*, vol. 17, no. 1, pp. 210–216, 2002.

[15] L. Liu, Z. Zhou, N. Dai, K.-W. Lao, and Y. Song, "Interpolated phase-shifted PWM for harmonics suppression of multilevel hybrid railway power conditioner in traction power supply system," *IEEE Transactions on Transportation Electrification*, vol. 8, no. 1, pp. 898–908, 2022.

[16] E. Mollerstedt and B. Bernhardsson, "Out of control because of harmonics-an analysis of the harmonic response of an inverter locomotive," *IEEE Control Systems Magazine*, vol. 20, no. 4, pp. 70–81, 2000.

[17] H. Hu, P. Pan, Y. Song, and Z. He, "A novel controlled frequency band impedance measurement approach for single-phase railway traction power system," *IEEE Transactions on Industrial Electronics*, vol. 67, no. 1, pp. 244–253, 2019.

[18] S. Mohammadi, A. V. Nadaraja, K. Luckasavitch, M. C. Jain, D. J. Roberts, and M. H. Zarifi, "A label-free, non-intrusive, and rapid monitoring of bacterial growth on solid medium using microwave biosensor," *IEEE Transactions on Biomedical Circuits and Systems*, vol. 14, no. 1, pp. 2–11, 2020.

[19] Y. Wang, H. E. Mazin, W. Xu, and B. Huang, "Estimating harmonic impact of individual loads using multiple linear regression analysis," *International Transactions on Electrical Energy Systems*, vol. 26, no. 4, pp. 809–824, 2016.

[20] Y. Sun, S. Li, Q. Xu, X. Xie, Z. Jin, F. Shi, and H. Zhang, "Harmonic contribution evaluation based on the distribution-level PMUs," *IEEE Transactions on Power Delivery*, vol. 36, no. 2, pp. 909–919, 2020.

[21] H. E. Mazin, W. Xu, and B. Huang, "Determining the harmonic impacts of multiple harmonic-producing loads," *IEEE Transactions on Power Delivery*, vol. 26, no. 2, pp. 1187–1195, 2011.

[22] E. Gursoy and D. Niebur, "Harmonic load identification using complex independent component analysis," *IEEE Transactions on power delivery*, vol. 24, no. 1, pp. 285–292, 2008.

[23] Y. Zhang, J. Lu, and J. Yong, “Harmonic damping characteristics of single-phase full-bridge rectifier based loads,” *CSEE Journal of Power and Energy Systems*, vol. 8, no. 5, pp. 1448–1456, 2022.

[24] S. Yang, Z. Shao, W. Zheng, and F. Chen, “Mitigation of background harmonics effect on MMC controller based on a novel coordinate transformation technique,” *IEEE Access*, vol. 7, pp. 167113–167126, 2019.

[25] H. Liao and D. Niebur, “Load profile estimation in electric transmission networks using independent component analysis,” *IEEE Transactions on Power Systems*, vol. 18, no. 2, pp. 707–715, 2003.

[26] F. Karimzadeh, S. Esmaeili, and S. H. Hosseinian, “A novel method for noninvasive estimation of utility harmonic impedance based on complex independent component analysis,” *IEEE Transactions on Power Delivery*, vol. 30, no. 4, pp. 1843–1852, 2015.

[27] J. Hui, W. Freitas, J. C. M. Vieira, H. Yang, and Y. Liu, “Utility harmonic impedance measurement based on data selection,” *IEEE Transactions on Power Delivery*, vol. 27, no. 4, pp. 2193–2202, 2012.

[28] F. Safargholi, K. Malekian, and W. Schufft, “On the dominant harmonic source identification—Part II: Application and interpretation of methods,” *IEEE Transactions on Power Delivery*, vol. 33, no. 3, pp. 1278–1287, 2018.

[29] S. Wang, H. Hui, Y. Ding, C. Ye, and M. Zheng, “Operational reliability evaluation of urban multi-energy systems with equivalent energy storage,” *IEEE Transactions on Industry Applications*, vol. 59, no. 2, pp. 2186–2201, 2023.

[30] H. Hui, Y. Chen, S. Yang, H. Zhang, and T. Jiang, “Coordination control of distributed generators and load resources for frequency restoration in isolated urban microgrids,” *Applied Energy*, vol. 327, p. 120116, 2022.

[31] Y. Chen, D. Qi, H. Hui, S. Yang, Y. Gu, Y. Yan, Y. Zheng, and J. Zhang, “Self-triggered coordination of distributed renewable generators for frequency restoration in islanded microgrids: A low communication and computation strategy,” *Advances in Applied Energy*, vol. 10, p. 100128, 2023.

[32] Q. Shi, H. Cui, F. Li, Y. Liu, W. Ju, and Y. Sun, “A hybrid dynamic demand control strategy for power system frequency regulation,” *CSEE Journal of Power and Energy Systems*, vol. 3, no. 2, pp. 176–185, 2017.

[33] H. Hui, P. Siano, Y. Ding, P. Yu, Y. Song, H. Zhang, and N. Dai, “A transactive energy framework for inverter-based HVAC loads in a real-time local electricity market considering distributed energy resources,” *IEEE Transactions on Industrial Informatics*, vol. 18, no. 12, pp. 8409–8421, 2022.

[34] R. Abu-Hashim, R. Burch, G. Chang, M. Grady, E. Gunther, M. Halpin, C. Harziadonin, Y. Liu, M. Marz, T. Ortmeyer, V. Rajagopalan, S. Ranade, P. Ribeiro, T. Sim, and W. Xu, “Test systems for harmonics modeling and simulation,” *IEEE Transactions on Power Delivery*, vol. 14, no. 2, pp. 579–587, 1999.

[35] *IEEE Recommended Practice and Requirements for Harmonic Control in Electric Power Systems*, IEEE Standard 519, 2014.

Shaohua Yang (Student Member, IEEE) received the B.Sc. degree from Hefei University of Technology, Hefei, China, in 2017 and the M.Sc. degree from Fuzhou University, Fuzhou, China, in 2020, both in electrical engineering. He is currently working toward the Ph.D. degree at University of Macau, Macao SAR, China. His research interests include cyber physical security, demand response, and power quality.

Keng-Weng Lao (Senior Member, IEEE) received his B.Sc., M.Sc., and Ph.D. degrees in electrical and electronics engineering from the Faculty of Science and Technology, University of Macau, Macau, China, in 2009, 2011, and 2016, respectively. He is currently an assistant professor with the Department of Electrical and Computer Engineering, as well as the State Key Laboratory of Internet of Things for Smart City, University of Macau. He was a Research Scholar in the Department of Electrical and Computer Engineering, The University of Texas at Austin, Austin, TX, USA from June 2017 to June 2019. His research interests include cyber-physical security, renewable energy integration, energy internet of things, smart energy system protection and smart grid. He was the recipient of the Macao Science and Technology Development Fund Postgraduate Award for Ph.D. Student 2016, first runner-up of the Challenge Cup National Intervarsity Science and Technology Competition 2013, and Championship of the Postgraduate Section in the IET Young Professionals Exhibition 2013.

Hongxun Hui (Member, IEEE) received the B.E. and Ph.D. degrees in electrical engineering from Zhejiang University, Hangzhou, China, in 2015 and 2020, respectively. From 2018 to 2019, he was a visiting scholar at the Advanced Research Institute in Virginia Tech, and the CURENT Center in University of Tennessee. He is currently a Research Assistant Professor with the State Key Laboratory of Internet of Things for Smart City, University of Macau, Macao SAR, China. His research interests include optimization and control of power system, demand response, and Internet of Things technologies for smart energy.

Yulin Chen (Member, IEEE) received the Ph.D. degree in Electrical Engineering from Zhejiang University, Hangzhou, China, in 2021. He was a Postdoctoral Fellow with University of Macau, Macao SAR, China, from September 2021 to September 2022. He is currently an Associate Research Fellow with Hainan Institute of Zhejiang University, Sanya, China. His current research interests include distributed control of renewable energy and cyber-physical security with application in smart grid.

Ningyi Dai (Senior Member, IEEE) received the B.Sc. degree in Electrical Engineering from Southeast University, Nanjing, China, in 2001, and the M.Sc. and Ph.D. degrees in Electrical and Electronics engineering from University of Macau, Macau, China, in 2004 and 2007, respectively. She is currently an Associate Professor with the Department of Electrical and Computer Engineering and SKL of Internet of Things for Smart City, University of Macau. She is also assistant Dean of Faculty of Science and Technology, University of Macau. She has authored or coauthored more than 80 technical journals and conference papers in power systems and power electronics. Her research interests include the application of power electronics in power systems, control of power converters and integrated energy system. Dr. Dai was the corecipient of the Macao Science and Technology Invention Award in 2012, 2018 and 2022.